Journal of Power Sources 315 (2016) 120–126

Contents lists available at ScienceDirect

Journal of Power Sources

journal homepage: www.elsevier.com/locate/jpowsour

One-step synthesis of hierarchically porous carbons for high-performance electric double layer supercapacitors

Haitao Zhang [a, **, 1], Lei Zhang [a, 1], Jun Chen [b, 1], Hai Su [a], Fangyan Liu [a], Weiqing Yang [a, *]

[a] Key Laboratory of Advanced Technologies of Materials (Ministry of Education), School of Materials Science and Engineering, Southwest Jiaotong University, Chengdu 610031, China
[b] School of Materials Science and Engineering, Georgia Institute of Technology, Atlanta, GA 30332, USA

HIGHLIGHTS

- HPCs with mass production are prepared by a one-step template-free method.
- Lower synthesis and manufacturing costs.
- HPCs based supercapacitors show superior electrochemical performances.
- Effect of pore structure on the electrochemical performances of HPCs is studied.

GRAPHICAL ABSTRACT

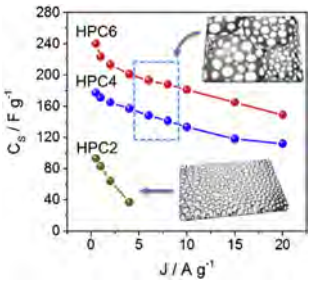

ARTICLE INFO

Article history:
Received 15 December 2015
Received in revised form
28 February 2016
Accepted 2 March 2016
Available online 19 March 2016

Keywords:
Supercapacitors
Hierarchically porous carbons
Neutral aqueous electrolytes
High performance

ABSTRACT

With plenty of unique porous structure at micro-/nano scale, hierarchically porous carbons (HPCs) are promising for usage in advanced electric double layer supercapacitors (EDLCs) as the electrode materials. However, wide-range adoption of HPC for practical application is largely shadowed by its extremely complex synthesis process with considerably low production efficiency. Herein we reported a simple template-free, one-step sintering method, to massively produce the HPCs for high-performance EDLCs. Resorting to the 3D structure modification of the wide pore size distribution, high surface area of HPCs (up to 3000 m^2 g^{-1}) was achieved. By using 1 M Na_2SO_4 as electrolyte, the as-fabricated HPCs based EDLCs can be operated reversibly over a wide voltage window of 1.6 V with superior specific capacitance of 240 F g^{-1} under a current density of 0.5 A g^{-1}. In the meanwhile, the EDLCs exhibit excellent rate capability (high power density of 16 kW kg^{-1} at 10.2 Wh kg^{-1}) and long-term cycling stability with 9% loss of its initial capacitance after 2000 cycles. This output performance distinguished itself among most of the carbon-based EDLCs with neutral aqueous electrolyte. Thus, the template-free one-step sintering method produced HPCs for EDLCs represents a new approach for high-performance energy storage.

1. Introduction

Based on the non-Faradaic processes, the electric double layer capacitors (EDLCs) have emerged an important type of device for next generation energy storage due to their fast charge/discharge rate and excellent cycling stability [1–3]. However, the EDLCs are suffering from far lower energy densities than that of the secondary

* Corresponding author.
** Corresponding author.
E-mail addresses: haitaozhang@swjtu.edu.cn (H. Zhang), wqyang@swjtu.edu.cn (W. Yang).
[1] H.T.Z., L.Z., and J.C. contributed equally to this work.

http://dx.doi.org/10.1016/j.jpowsour.2016.03.005
0378-7753/

batteries, such as lead-acid batteries and lithium-ion batteries.

Theoretically, according to $E = C_S V^2/2$, the enhancement of energy density (E) of EDLCs can be achieved by maximizing both the specific capacitance (C_S) and the voltage window (V). Experimentally, a variety of strategies were attempted in the past ten years, including intrinsic structure design to increase the specific capacitance [4,5], assembling asymmetric and hybrid structured devices [6,7]; developing the electrolytes with high voltage window [8,9]; The EDLCs with strong acid/alkali aqueous electrolytes indeed exhibit much higher C_S, however, they suffer from narrow voltage window, which can only operate in a voltage of 1.0 V due to the limitation of the water decomposition. And this design was also challenged due to its potential environmental pollution. A promising direction is to design environmentally friendly materials that have outstanding electrochemical properties in salt aqueous electrolytes like Na_2SO_4 and Li_2SO_4 with the merits of high ionic conductivity, high voltage window (up to 1.5–2.0 V), safety, non−corrosiveness and convenient assembly in air [10–12].

Hierarchically porous carbons (HPCs) are such a good candidate and electrochemically stable within a wide range of operating voltage [13–17]. However, most of HPCs were generally fabricated by using hard or soft template-based methods, which required very much complex synthesis procedures with considerably low mass production [18–22]. In hard templating, infiltration of the carbon precursors into the pores of $Ni(OH)_2$ [20] the silica [21], or zeolite templates [22] was carried out, followed by a carbonization treatment and finally the removal of the template to get the template-free porous carbon replica. Thus, to solve this, developing template-free method for the preparation of HPCs materials are critical [23,24], however, it still exists a big challenge.

Here in this work, we reported a simple and effectively template-free method to prepare HPCs based on one-step carbonization and activation of Polyvinylidene Fluoride (PVDF) with molten KOH. By extracting the fluorine element from PVDF and reassembling the C−C bond, the obtained HPCs possess high ratio of micropores, mesopores, and high mass of KOH generated macropores with a high SSA of 3003 $m^2\ g^{-1}$, large pore volume of 2.27 $cm^3\ g^{-1}$, as well as a wide pore size distribution. And these superior features well serve as the EDLC electrode materials and a maximum specific capacitance of 60 F g^{-1} (240 F g^{-1} for a single electrode) with an energy density of 21.2 Wh kg^{-1} has been obtained. In 1 M Na_2SO_4 aqueous electrolyte, the as-developed EDLCs can also be operated reversibly over a wide voltage window of 1.6 V. To date, this output performance is the highest value reported for the hierarchically porous carbons as well as mesoporous carbons based EDLCs with neutral aqueous electrolytes [10,25,26]. Moreover, the HPC-based EDLCs exhibited good rate-capability and also possessed long-term cycling stability with 91% retention after 2000 cycles. These observations unambiguously demonstrate the capability of the template-free one-step processed HPCs as high-performance electrode materials for EDLCs with neutral aqueous electrolytes, which opens up a new approach for high-performance energy storage and is suited for mass production.

2. Experimental

2.1. Synthesis of HPC samples

HPCs were synthesized by directly sintering process. Both the PVDF and KOH were used as precursors to prepare HPCs. The PVDF powder was purchased from Arkema (HSV900, French), and its molecular weight is 800,000–1,000,000 g mol^{-1}. The weight ratio of KOH to PVDF was controlled in a range from 2:1 to 6:1. The samples were prepared from carbonization and activation of PVDF using different amounts of KOH, namely, HPC2, HPC4, and HPC6. Take the synthesis of HPC6 as an example, 2.5 g PVDF and 15.0 g KOH were added into a Ni crucible. And then put them into a horizontal tube furnace (Φ 60 × 1200 mm, SGSL-1600×, Hefei Kejing Materials Technology CO., LTD, China). The furnace was heated to 380 °C and retained this temperature for 2 h to melt the KOH. Followed by a sequentially heating to 800 °C and stayed for 2 h. The resultants were cooled down to room temperature naturally. All the chemical reactions were preceded under a 160 sccm flowing Ar gas. After the reaction, the products were sonicated in 6 M HCl for 20 min, and then they were washed ordinarily with deionized water and alcohol to remove impurities. The obtained yields for HPC2, HPC4, and HPC6 were about 0.15, 0.45, and 0.68 g, respectively.

2.2. Sample characterization

Scanning electron microscopy (SEM) was carried out on Zeiss Sigma scanning electron microscopes. Energy dispersive X-ray spectroscopy (EDX) was carried out on an EDAX TEAM EDS. Transmission electron microscopy (TEM) and high-resolution TEM (HRTEM) characterizations were performed with a JEOL JSM-2010 operating at an accelerating voltage of 200 kV. X-ray diffraction (XRD) of the samples was performed with D8 Advance diffractometer with Cu radiation between 5 and 70°. Room-temperature Raman spectra were obtained with a RM2000 microscopic confocal Raman spectrometer with a 514 nm laser beam. X-ray photoemission microscopy (XPS) analysis was carried out with a PHI Quantear SXM (ULVAC-PHINC). Brunaue−Emmertt−Teller (BET) surface areas and density functional theory (DFT) pore size distribution measurements of HPCs were performed with Micromeritics ASAP 2020 surface area and pore size analyzer using nitrogen gas adsorption-desorption isotherm at −196 °C.

2.3. Electrochemical measurements

For assembling EDLCs, 2032 type coin cells were used. 85 wt% of the HPCs, 8 wt% conductive agent (Super C45, Timcal) and 7 wt% Polytetrafluoroethylene (PTFE, Sigma Aldrich) binder were mixed in isopropyl alcohol, and blended for 30 min before using. The obtained slurry was heated at 80 °C to remove excess isopropanol and then kneaded thoroughly and rolled down to shape it into 100–120 μm thick films. After drying for 24 h at 120 °C, the films punched into 1.1 cm diameter electrodes and the mass of a single electrode for HPC2, HPC4, and HPC6 are about 9, 6.5 and 4 mg, respectively. The as-rolled tape densities of HPC2, HPC4, and HPC6 electrodes are 0.79 ± 0.02, 0.60 ± 0.03, 0.42 ± 0.02 g cm^{-3}, respectively. Then the HPC disks were pressed onto nickel foam and the electrode plates were further mechanically compacted. A cellulose separator (F4050, NKK) was sandwiched between two electrodes to fabricated symmetrical supercapacitors and 1 M Na_2SO_4 and 6 M KOH were employed as the electrolytes.

The cyclic voltammetry (CV) curves and electrochemical impedance spectroscopy (EIS) were carried out by using the electrochemical workstation (CHI660E). And EIS was obtained in the frequency range from 100 kHz to 10 mHz. The galvanostatic charge-discharge (GCD) process and cycle-life test of EDLCs were measured on an Arbin MSTAT4 multi-channel galvanostat/potentiostat instrument. The specific capacitance of EDLC electrodes can be calculated as:

$$C_S = I\Delta t \Big/ \Delta U m \left(\mathrm{F\ g^{-1}}\right) \quad (1)$$

where I, Δt, ΔU and m are respectively the applied current, the discharge time, the potential window after IR drop and the total

active mass of both electrodes without including the binders and the conductive agents.

The energy density (E), effective power density (P_{eff}), and the maximum power density (P_{max}) can be evaluated by using the following equations:

$$E = C_S \Delta U^2 \Big/ (2 \times 4 \times 3.6) \left(\mathrm{Wh\ kg^{-1}}\right) \quad (2)$$

$$P_{eff} = 3.6 \times E/t \left(\mathrm{kW\ kg^{-1}}\right) \quad (3)$$

$$P_{max} = V^2 \Big/ (4 \times EDR \times m) \left(\mathrm{kW\ kg^{-1}}\right) \quad (4)$$

where EDR is the equivalent distributed resistance. All of the values were normalized with respect to the combined weight of both electrodes.

3. Results and discussion

The sintering process of preparing PVDF into hierarchically porous carbon particles is schematically illustrated in Fig. 1a. When the KOH was loaded onto the PVDF with a mass ratio of 2:1, the carbon materials (HPC2) are wrinkled sheets with carbon particles of several micrometers. The related morphologies of HPC2 are shown in Supporting Figs. S1a and S1b. With increasing the mass ratio of KOH to 4:1 and 6:1, the activation degree of samples are increased. The obtained HPC4 and HPC6 contain various macropores and numerous small-sized micropores, as shown by Fig. 1b for HPC4 and Fig. 1c and d for HPC6. With regard to this, we will further discuss in the next section on TEM characterization and surface area analysis. As a consequence, the HPC6 and HPC4 hold a

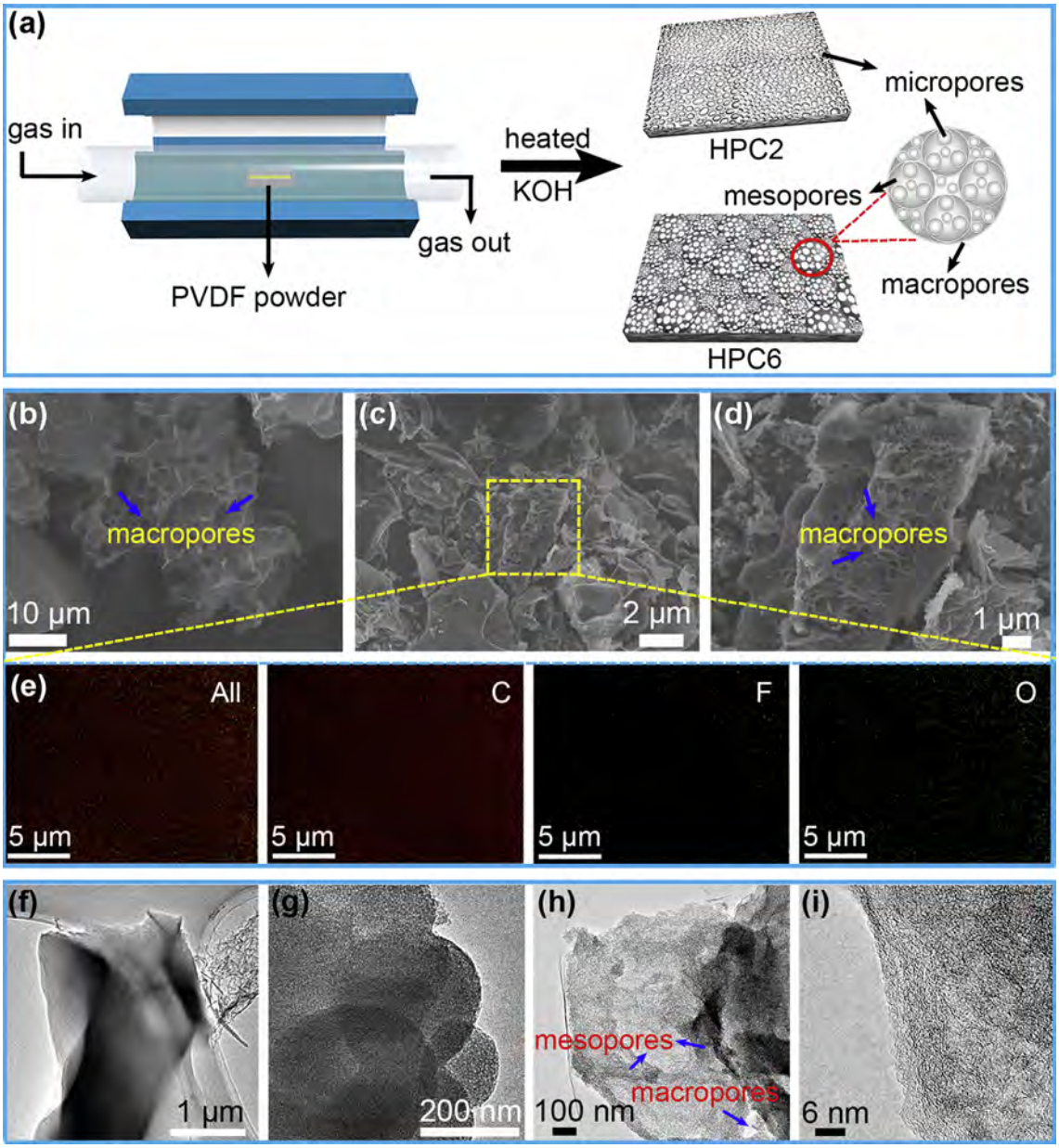

Fig. 1. (a) A schematic illustration of the sintering process for preparing PVDF into hierarchically porous carbon particles. SEM images of HPCs, (b–c) HPC6, (d) HPC4, and (e) EDX mapping of HPC6. TEM images of (f) HPC2, (g) HPC4, (h) HPC6 samples, and (i) HRTEM images of HPC6.

hierarchical micro-, meso-/macroporous structure with good pore connectivity. After sintering, the Fluorine atoms are greatly eliminated from the PVDF, and the obtained HPCs have high ratio of Carbon atoms, which was proved by the sample EDX detection, as shown in Fig. 1e. And the atomic ratio of Carbon and Oxygen in the as-fabricated HPC6 sample is 95.5% and 4.5%, respectively. The traces of Fluorine and Potassium atoms are less than 0.1%.

The TEM images of HPC and the (0 0 2) lattice fringe mode show that the material is heterogeneous (Fig. 1f–i). HPC2 is composed of carbon block and sheet like carbons as shown in Fig. 1f. The main characteristic of HPC4 and HPC6 is the presence of many mesopores and hierarchical carbon bulk as shown in Fig. 1g and h. Since HPC samples are produced including KOH activation process, the crystallinity of HPC samples show amorphous structure as indicated by HRTEM characterization (HPC6 of Fig. 1i, HPC2 and HPC4 are similar, Supporting Fig. S2).

XRD results also illustrate that HPCs lose long-range ordered graphite structure (Fig. 2a). In fact, the effective crystallite size L_a in the direction of the graphite plane is only about 1.5~2.0 nm by Raman spectroscopy characterization using the multi-peak fit with a R^2 value of >0.998, as shown in Fig. 2b and Supporting Fig. S3. The C 1s spectrum is dominated by the C–C species at 284.5 eV as illustrated in Fig. 2c. Some additional minor components at a higher binding energy are presented, which can be assigned to O1s and O KLL. The traces of Fluorine and Potassium atoms are negligible, which is also supported by full scan spectrum detection of XPS. A XPS deconvolution spectrum of C1s in Fig. 2d indicates that HPCs are dominant sp^2 carbon with oxygen functionalized carbon atoms, including C–OH, epoxy C, and C=O. The atomic ratio of Carbon and Oxygen are 94.8% and 5.2% for HPC6, which are similar to the results of EDX mapping characterization.

N_2 adsorption and desorption isotherms of the HPCs was further performed to investigate the SSA and pore size distribution, which is highly related to their electrochemical properties [27]. As demonstrated in Fig. 3a, the as-fabricated HPCs show a representative type IV isotherm with a H2 hysteresis loop at relative pressures (P/P_0) of 0.45–0.85, indicating clear capillary condensation derived from mesopores inside the HPCs. Given a constant of the sintering temperature, the specific surface area (SSA), pore size distribution (PSD) and pore volume of HPCs are significantly influenced by the mass ratio of KOH. Namely, with an increased mass ratio of the KOH loading on PVDF, the SSA was dramatically increased reaching a highest value of 3003 $m^2\ g^{-1}$ for HPC6. Meanwhile, as the KOH concentration increases, the pore volume of the HPCs increases from 0.52 $cm^3\ g^{-1}$ (HPC2) to 1.45 $cm^3\ g^{-1}$ (HPC4) and further to 2.27 $cm^3\ g^{-1}$ (HPC6). Fig. 3b displays the DFT PSD of the HPCs, which justified the effectiveness of introducing microporoes and mesoporoses on the HPCs by a one-step sintering process in the presence of KOH. The HPC2 show a dominant pore size distribution less than 2 nm. With increasing the KOH mass, a much more porous structure emerges in both the HPC6 and HPC4. And the mesopores ~3 nm is also largely increased, which provide low resistant ionic pathway, improving the accessibility of micropores to electrolytes. Moreover, micropores less than 2 nm are greatly increased for HPC6 and HPC4 samples, as exhibited in Fig. 3b. The variety of pore sizes with high pore volume can not only provide highly efficient mass transport through mesopores but also a large SSA from the micro-to meso-pores, thus to achieve excellent performances for EDLC applications.

To fully utilize the porous structure of HPCs, a further step was taken to develop it into symmetric EDLCs as the electrodes materials. In the test, we also employed the 1 M Na_2SO_4 as the electrolyte. Fig. 4a exhibits CV curves of the EDLCs made from HPC6 at voltage windows of 1.2, 1.4, 1.6, and 1.8 V at a scan rate of 10 mV s^{-1}.

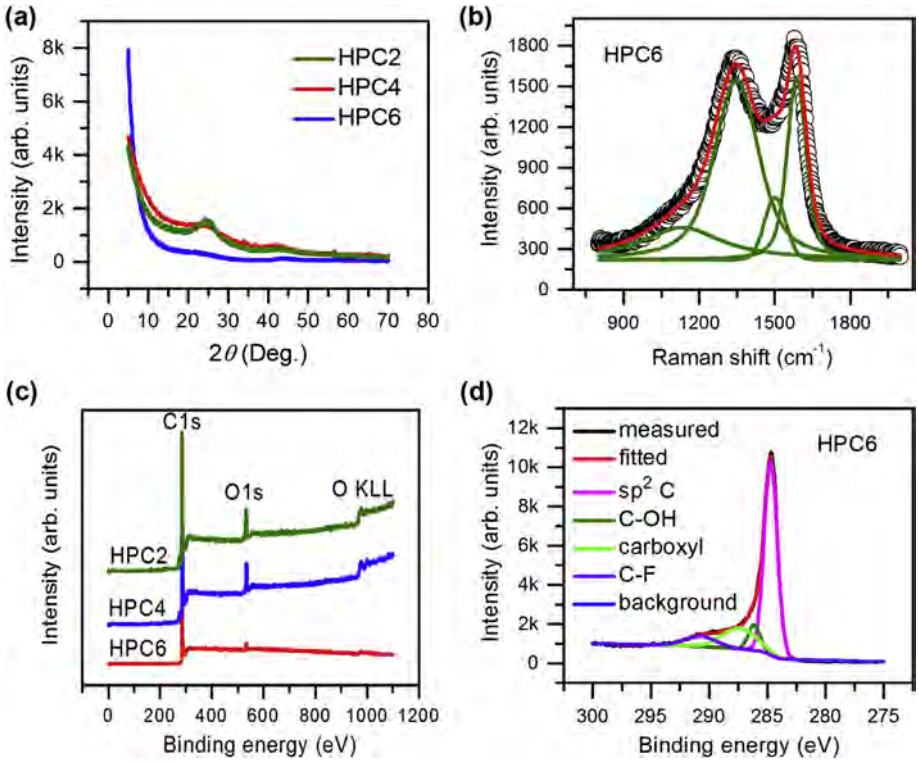

Fig. 2. HPCs characterizations. (a) XRD patterns of HPCs. (b) Raman spectra of HPC6. (c) XPS full-scan spectra of HPCs and (d) C1s spectrum of HPC6. These characterizations indicate that the fluorine elements are mostly extracted from the Polyvinylidene Fluoride powders and the remained C–C bonds are transformed into HPCs through a simple and effectively template-free method based on one-step carbonization and activation of Polyvinylidene Fluoride with molten KOH.

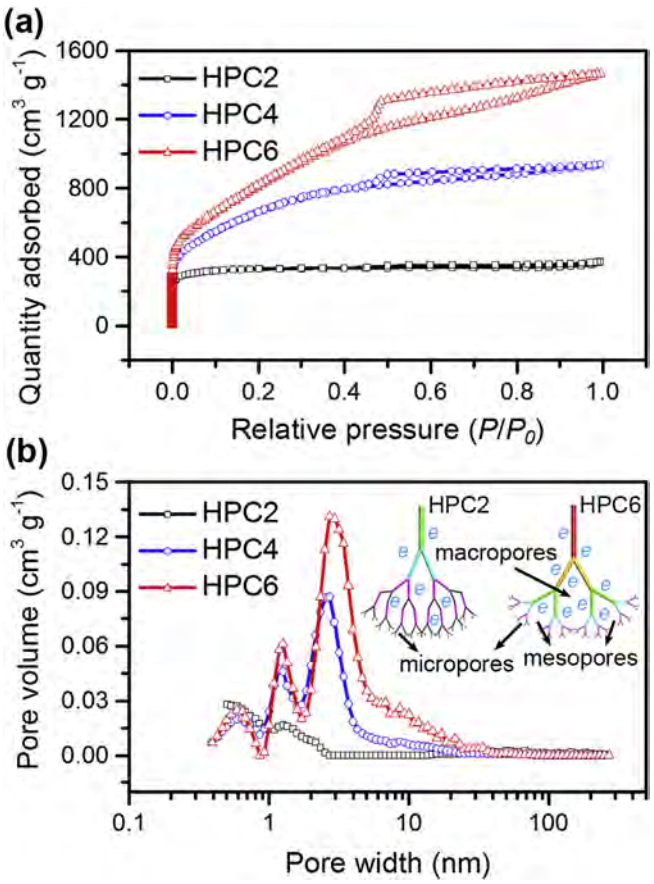

Fig. 3. (a) N_2 adsorption/desorption isotherms and (b) pore size distribution of the HPCs. The inset illustrates the pore structure. The specific surface area and the pore volume of hierarchically porous carbons reach up to 3003 $m^2\ g^{-1}$ and 2.27 g cm^{-3}, respectively. The peak positions calculated by density functional theory model locate at about 0.6, 1.2, and 3.0 nm, which unambiguously demonstrate the effectiveness of introducing microporoes and mesoporoses on the HPCs by a one-step template-free method.

The fabricated EDLCs showed an ideal capacitive behavior with rectangular CV curves, even at the voltage window up to 1.6 V. However, when the EDLCs were tested at a high voltage of 1.8 V, the CV curves showed a distortion behavior at high voltages around 1.6–1.8 V. This limitation is attributed to the decomposition of electrolyte with hydrogen and/or oxygen evolution. Although higher voltage output of the EDLCs provides advantages of reducing the devices number connected in series to obtain the desired output voltage, the coulombic efficiency, energy efficiency, and the cycling stability would be significantly deteriorated. Previous work proved that the carbon/carbon EDLCs in neutral aqueous electrolyte displayed an accelerated aging under a high voltage window [28]. As a result, to further investigate the overall electrochemical performances of the as-fabricated HPC-based EDLCs, we set the potential window of 1.6 V with 1 M Na_2SO_4 as the aqueous electrolyte.

The CV curves of different HPC samples at a scan rate of 20 mV s^{-1} are shown in Supporting Fig. S4a. Both HPC4 and HPC6 based EDLCs show a rectangular shape, indicating a good capacitive behavior. While the HPC2 based EDLC display a distorted shape at both low and high voltage ranges, which is mainly attributed to the inferior capacitive behavior of the HPC2 sample. Namely, the micropores inside the HCP2 carbon hindered the transportation of the salt aqueous electrolyte ions. The CV curves of HPC4 based EDLCs at different scan rates of 20–300 mV s^{-1} between 0 and 1.6 V were shown in Supporting Fig. S4b. CV profiles still retain a rectangular shape without obvious distortion with increasing potential scan rates, even up to a scan rate of 200 mV s^{-1}. This capability exhibits an excellent charge/discharge rate of the EDLC as practical power sources.

Fig. 4b presents the specific capacitance obtained from the GCD curves of the HPC electrodes. And the HPC6 and HPC4 based EDLCs exhibit higher capacitance and better power capability compared to that of based on HPC2. A maximum specific capacitance of 60 F g^{-1} was obtained from the HPC6 EDLC based on two symmetrical electrodes at a current density of 0.5 A g^{-1}, which equals to 240 F g^{-1} for a single electrode. This achievement is much higher than most of the carbon materials based EDLCs, and even superior to many pseudo-capacitive materials, like MnO_2 based supercapacitors with neutral aqueous electrolytes [11,29–33]. To distinguish, the specific capacitances of HPC materials, porous carbons and MnO_2 were tabulated in Supporting Table S1. Moreover, the HPC6 and HPC4 show high rate-capability. The specific capacitances of HPC6 and HPC4 based EDLCs were calculated to be 60 and 44.3 F g^{-1} at 0.5 A g^{-1}, and still maintaining capacitances of 44.3 and 28 F g^{-1} when the EDLCs are operated at a fast charge/discharge of 20 A g^{-1}, demonstrating high retentions up to 62% and 63%, respectively. The enhancement of the specific capacitance and rate capability of HPCs can be attributed to firstly, the high EDL capacitances due to the high SSA and large pore volume of HPC6 and HPC4, and secondly, the hierarchically porous structure that exhibiting short diffusion path lengths for both electrolyte ions and electrons, favoring fast diffusion of electrolyte ions during the GCD process. The GCD curves in a potential window of 0–1.6 V at a current density of 0.5 A g^{-1} was presented in Supporting Fig. S5a. And the GCD curves at the different current densities are presented in Supporting Fig. S5b. The symmetric charge-discharge curves in the whole potential range also demonstrate an EDL capacitance in nature. In addition, the coulombic efficiency of HPC4 and HPC6 electrodes reaches up to 95% and 93% at the current density of 0.5 A g^{-1}, which also proves that the voltage window of 1.6 V is compatible with HPC-based EDLCs. HPC6 based EDLCs show high specific capacitance of 50.3, 47.0 and 37.3 F g^{-1} at 4, 8, and 20 A g^{-1}, respectively. At higher current densities, HPC-based EDLCs show an apparent voltage (*IR*) drop, which is attributed to the equivalent series resistance (*ESR*).

The power capability of EDLCs depends strongly on the equivalent *ESR* and the *EDR*. In the meanwhile, the EIS is an effective method to evaluate the two parameters. In this regard, the EIS of the HPCs based EDLCs was plotted in Fig. 4c. It clearly shows that the HPC4 and HPC6 electrodes exhibit a vertical line at the low frequency, indicating a good EDL capacitance. The *ESR* and *EDR* are respectively 1.0, 1.7 Ω for HPC4 and 1.1, 2.5 Ω for HPC6 based EDLCs, which are determined by using a method suggested by R. Kötz et al. [34]. Accordingly, the maximum power density is calculated to be 30 and 31 kW kg^{-1} for the HPC4 and HPC6 based EDLCs, owing to the enhanced ions transfer efficiency resulted from 3D interconnected carbon framework and hierarchical pores in the carbon materials. The *ESR* of HPC-based EDLCs with neutral aqueous electrolytes is relatively low. However, these *ESRs* are still quite larger than those with strong acid/alkali aqueous electrolytes, which ascribes to two reasons. On one hand, neutral electrolytes have low electrical conductivity. On the other hand, the viscosity and electrolyte ions are larger in salt electrolytes. Here we also prove that HPC6 electrodes have low *ESR* and show excellent power capability with 6 M KOH electrolytes, as demonstrated in Supporting Fig. S6. To contrast, HPC2 electrodes show extremely large diffusion resistance, which can also result from its low pore volume and dominant microporous size.

For a systematical investigation, as one of the most critical factors, a further step was taken to evaluate the cycling stability of the

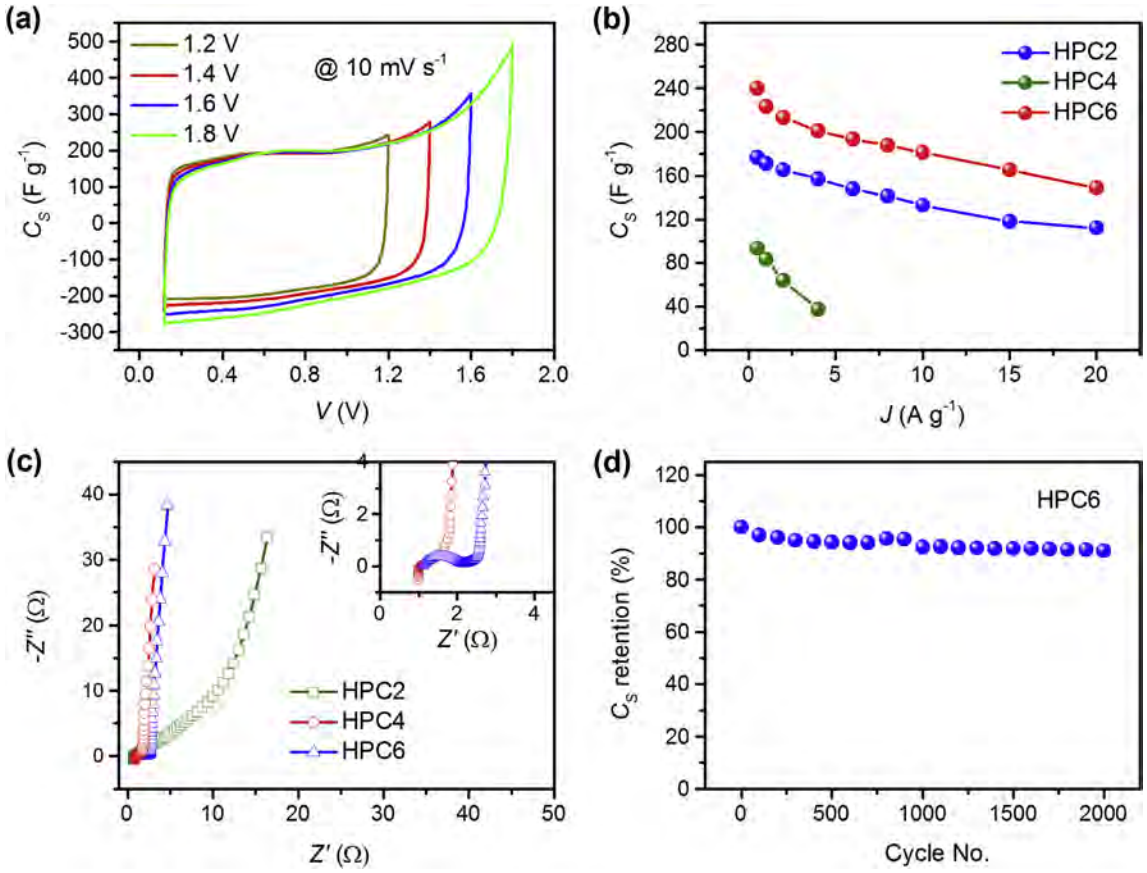

Fig. 4. The electrochemical performances of HPC-based EDLCs. (a) The CV curves of HPC-based EDLCs in a voltage window of 1.2–1.8 V at a scan rate of 10 mV s^{-1}. (b) A comparison of the specific capacitance of HPC-based EDLCs at different GCD current densities. (c) Nyquist plots of HPC-based EDLCs; the inset shows the enlarged part of Nyquist plots at high frequency. (d) The cycling stability of HPC6 EDLCs, the inset shows Nyquist plots at high frequency before and after cycling.

HPC-based EDLCs in 1 M Na_2SO_4 with a voltage window of 1.6 V. As shown in Fig. 4d, at a high current density of 5 A g^{-1}, the HPC6 based EDLCs show 91% capacitance retention over 2000 cycles. The inset of Fig. 4d presents a comparison of the EIS plots of HPC6 electrodes before and after 2000 cycles. And the diameters of the semicircles increase slightly after 2000 cycles. In addition, the *EDR* of the HPC6 electrodes are measured to be about 2.9 Ω by extrapolating the straight line to intersect at the real axis, which indicates an increasing of 16% after 2000 cycles.

Fig. 5 shows the Ragone plots of the HPC-based EDLCs in the potential range of 0–1.6 V. The HPC6 based EDLCs could deliver a maximum energy density up to 21.2 Wh kg^{-1}, higher than that of 15.5 and 7.9 Wh kg^{-1} respectively for HPC4 and HPC2 based EDLCs. This output performance is higher than the majority of previously reported symmetric carbon based EDLCs and even comparable with many asymmetrical supercapacitors [7,10,32,35,36]. Moreover, consisting of Faradaic pseudocapacitance reactions, the asymmetrical supercapacitors could lead to undesirable leakage currents and device degradation with cycling and/or storage, particularly at elevated temperatures. The energy densities of 14.2 and 10.2 Wh kg^{-1} were maintained for HPC6 based EDLCs when the power densities increased to 8 and 16 kW kg^{-1}. To justify the HPC based EDLC as a practical power source, two HPC6 based EDLCs was connect in series to form a power package, and it was charged at a current density of 1 A g^{-1} and then holding at the voltage of 3.2 V for 600 s. A display board consisted of about 400 LEDs was lighted up simultaneously by the power package for 4 s (Fig. S7 and Supporting Movie S1). The demonstration sufficiently proves the superior performance of HPCs based EDLCs for energy storage and as practical portable power sources.

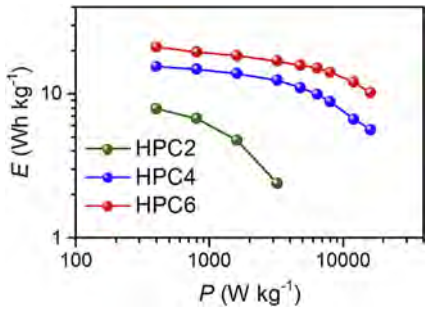

Fig. 5. Ragone plots of the HPC-based EDLCs.

Supplementary video related to this article can be found at http://dx.doi.org/10.1016/j.jpowsour.2016.03.005.

4. Conclusions

To summarize, we creatively invented a one-step sintering method to prepare the HPCs, which is also suitable for mass production. And a series of HPCs with unique features were fabricated and systematically characterized. With a mixed conducting 3D network, the synthesized HPCs hold a high SSA up to 3000 m^2 g^{-1}, large pore volume of 2.27 cm^3 g^{-1} and good pore size distribution. When the HPCs were used as the EDLC electrode material in neutral

aqueous electrolyte, a maximum specific capacitance of 240 F g^{-1}, good rate-capability and long cycling ability were achieved in this comprehensive study. The HPCs-based EDLCs can be operated reversibly in a wide potential window up to 1.6 V and delivers a high energy density of 21.2 Wh kg^{-1} along with a high power density of 16 kW kg^{-1}. These electrochemical performances will distinguish of the HPCs as electrode materials for high performance EDLCs. The present reported one-step sintering method paves the way to simply produce template-free hierarchically porous carbons and opens up a new approach for high-performance energy storage.

Acknowledgement

This work is supported by the National Natural Science Foundation of China (No. 51202023) and the scientific and technological projects for distinguished young scholars of Sichuan Province (No. 2015JQ0013).

Appendix A. Supplementary data

Supplementary data related to this article can be found at http://dx.doi.org/10.1016/j.jpowsour.2016.03.005.

References

[1] J.R. Miller, P. Simon, Science 321 (2008) 651–652.
[2] J. Vatamanu, D. Bedrov, J. Phys. Chem. Lett. 6 (2015) 3594–3609.
[3] X. Zhang, H.T. Zhang, C. Li, K. Wang, X.Z. Sun, Y.W. Ma, RSC Adv. 4 (2014) 45862–45884.
[4] M.F. El-Kady, V. Strong, S. Dubin, R.B. Kaner, Science 335 (2012) 1326–1330.
[5] H. Jiang, P.S. Lee, C. Li, Energ. Environ. Sci. 6 (2013) 41–53.
[6] X.Z. Sun, X. Zhang, H.T. Zhang, N.S. Xu, K. Wang, Y.W. Ma, J. Power Sources 270 (2014) 318–325.
[7] S. Wu, W. Chen, L. Yan, J. Mater. Chem. A 2 (2014) 2765.
[8] H.T. Zhang, X. Zhang, X.Z. Sun, D.C. Zhang, H. Lin, C.H. Wang, H.J. Wang, Y.W. Ma, ChemSus Chem. 6 (2013) 1084–1090.
[9] M. Armand, F. Endres, D.R. MacFarlane, H. Ohno, B. Scrosati, Nat. Mater. 8 (2009) 621–629.
[10] Q. Wang, J. Yan, Y. Wang, T. Wei, M. Zhang, X. Jing, Z. Fan, Carbon 67 (2014) 119–127.
[11] J.-G. Wang, Y. Yang, Z.-H. Huang, F. Kang, Carbon 61 (2013) 190–199.
[12] B. Dyatkin, V. Presser, M. Heon, M.R. Lukatskaya, M. Beidaghi, Y. Gogotsi, ChemSus Chem. 6 (2013) 2269–2280.
[13] E. Frackowiak, F. Beguin, Carbon 39 (2001) 937–950.
[14] P. Simon, Y. Gogotsi, Nat. Mater. 7 (2008) 845–854.
[15] A. Ghosh, Y.H. Lee, ChemSus Chem. 5 (2012) 480–499.
[16] H.T. Zhang, X. Zhang, X.Z. Sun, Y.W. Ma, Sci. Rep. 3 (2013).
[17] H.T. Zhang, K. Wang, X. Zhang, H. Lin, X.Z. Sun, C. Li, Y.W. Ma, J. Mater. Chem. A 3 (2015) 11277–11286.
[18] Y.S. Hu, P. Adelhelm, B.M. Smarsly, S. Hore, M. Antonietti, J. Maier, Adv. Funct. Mater. 17 (2007) 1873–1878.
[19] J. Gorka, M. Jaroniec, J. Phys. Chem. C 114 (2010) 6298–6303.
[20] D.W. Wang, F. Li, M. Liu, G.Q. Lu, H.M. Cheng, Angew. Chem. Int. Ed. 48 (2009), 1525–1525.
[21] Y. Han, X.T. Dong, C. Zhang, S.X. Liu, J. Power Sources 227 (2013) 118–122.
[22] K. Kim, M. Choi, R. Ryoo, Carbon 60 (2013) 175–185.
[23] S.J. Yang, T. Kim, K. Lee, Y.S. Kim, J. Yoon, C.R. Park, Carbon 71 (2014) 294–302.
[24] S. Chao, Q. Cui, K. Wang, Z. Bai, L. Yang, J. Qiao, J. Power Sources 288 (2015) 128–135.
[25] W. Gu, M. Sevilla, A. Magasinski, A.B. Fuertes, G. Yushin, Energ. Environ. Sci. 6 (2013) 2465.
[26] S. Song, F. Ma, G. Wu, D. Ma, W. Geng, J. Wan, J. Mater. Chem. A 3 (2015) 18154–18162.
[27] A.G. Pandolfo, A.F. Hollenkamp, J. Power Sources 157 (2006) 11–27.
[28] P. Ratajczak, K. Jurewicz, P. Skowron, Q. Abbas, F. Béguin, Electrochim. Acta 130 (2014) 344–350.
[29] Q.T. Qu, B. Wang, L.C. Yang, Y. Shi, S. Tian, Y.P. Wu, Electrochem. Commun. 10 (2008) 1652–1655.
[30] E.G. Calvo, F. Lufrano, P. Staiti, A. Brigandì, A. Arenillas, J.A. Menéndez, J. Power Sources 241 (2013) 776–782.
[31] X. Yang, Y.-S. He, G. Jiang, X.-Z. Liao, Z.-F. Ma, Electrochem. Commun. 13 (2011) 1166–1169.
[32] J.P. Li, Z.H. Ren, Y.Q. Ren, L. Zhao, S.G. Wang, J. Yu, RSC Adv. 4 (2014) 35789–35796.
[33] G. Yu, L. Hu, M. Vosgueritchian, H. Wang, X. Xie, J.R. McDonough, X. Cui, Y. Cui, Z. Bao, Nano Lett. 11 (2011) 2905–2911.
[34] D. Weingarth, D. Cericola, F.C.F. Mornaghini, T. Hucke, R. Kötz, J. Power Sources 266 (2014) 475–480.
[35] H. Gao, F. Xiao, C.B. Ching, H. Duan, ACS Appl. Mater. Inter. 4 (2012) 2801–2810.
[36] Y. Liu, D. He, H. Wu, J. Duan, Y. Zhang, Electrochim. Acta 164 (2015) 154–162.